

## Numerical Simulation of Internal Kelvin Waves and Coastal Upwelling Fronts\*

DMITRY BELETSKY AND WILLIAM P. O'CONNOR

*Cooperative Institute for Limnology and Ecosystems Research, University of Michigan, Ann Arbor, Michigan*

DAVID J. SCHWAB

*NOAA Great Lakes Environmental Research Laboratory, Ann Arbor, Michigan*

DAVID E. DIETRICH

*Center for Air Sea Technology, Mississippi State University, Stennis Space Center, Mississippi*

(Manuscript received 26 September 1995, in final form 2 May 1996)

### ABSTRACT

Two three-dimensional primitive equation numerical ocean models are applied to the problem of internal Kelvin waves and coastal upwelling in the Great Lakes. One is the Princeton Ocean Model (POM) with a terrain-following ( $\sigma$ ) vertical coordinate, and the other is the Dietrich/Center for Air Sea Technology (DIECAST) model with constant  $z$ -level coordinates. The  $\sigma$  coordinate system is particularly convenient for simulating coastal upwelling, while the  $z$ -level system might be better for representing abrupt topographic changes. The models are first tested with a stratified idealized circular lake 100 km in diameter and 100 m deep. Two bottom topographies are considered: a flat bottom and a parabolic depth profile. Three rectilinear horizontal grids are used: 5, 2.5, and 1.25 km. The POM was used with 13 vertical levels, while the DIECAST model was tested with both 13 and 29 vertical levels. The models are driven with an impulsive wind stress imitating the passage of a weather system.

In the case of the flat-bottom basin, the dynamical response to light wind forcing is a small amplitude internal Kelvin wave. For both models, the speed of the Kelvin wave in the model is somewhat less than the inviscid analytic solution wave speed. In the case of strong wind forcing, the thermocline breaks the surface (full upwelling) and a strong surface thermal front appears. After the wind ceases, the edges of this thermal front propagate cyclonically around the lake, quite similar to an internal Kelvin wave. In the case of parabolic bathymetry, Kelvin wave and thermal front propagation is modified by interaction with a topographic wave and a geostrophic circulation. In both models, higher horizontal resolution gives higher wave and frontal speeds. Horizontal resolution is much more critical in the full upwelling case than in the Kelvin wave case. Vertical resolution is not as critical.

The models are also applied to Lake Michigan to determine the response to strong northerly winds causing upwelling along the eastern shore. The results are more complex than for the circular basin, but clearly show the characteristics of cyclonically propagating thermal fronts. The resulting northward warm front propagation along the eastern shore compares favorably with observations of temperature fluctuations at municipal water intakes after a storm, although the model frontal speed was less than the observed speed.

### 1. Introduction

Large lakes are particularly interesting dynamically because they are subject to many of the same forcings as coastal oceans, have both nearshore and midlake dynamical regimes, and have a variety of associated mesoscale phenomena (Csanady 1984). They are easier to study than the coastal ocean because they are smaller and do not have salinity effects or tides. It is also not

necessary to specify open boundary conditions in lakes, as it is for the coastal ocean. For many environmental problems in the Great Lakes and in the coastal ocean, it is necessary to know the time-dependent three-dimensional temperature distribution and circulation, which is frequently dominated by wind-induced upwelling and coastally trapped waves (Wang and Mooers 1976; Clarke 1977; Wang 1982). Therefore, a better understanding of these processes will provide better predictions in both environments.

The thermal structure and circulation of the Great Lakes depend greatly on the season because of the large annual variation in surface heat flux (Boyce et al. 1989). In summer and fall there is a distinct thermocline in the upper 30 m in most of the lakes. The upper 5–15 m above the thermocline is usually well mixed by the wind in the temperature range 15°–20°C. In the thermocline,

---

\*Great Lakes Environmental Research Laboratory Contribution Number 973.

---

Corresponding author address: Dr. David J. Schwab, NOAA/ERL/GLERL, 2205 Commonwealth Blvd., Ann Arbor, MI 48105-1593.

the temperature can decrease to 5°–6°C around depths of 30 m. Below this depth the temperature remains nearly isothermal (Murthy and Schertzer 1994).

During the period of stratification, significant wind events will cause upwelling of the thermocline along the shore. Upwelling generally occurs on the upwind shore and the shore to the left of the wind direction, as discussed by Csanady (1968). These wind forcings, directly or through Ekman drift, move surface water away from the shore so that it must be replaced by colder upwelled water. In Lake Michigan, because of its north-south orientation, upwelling occurs along the eastern shore as a result of northerly winds, and along the western shore with southerly winds. This process can cause the nearshore lake temperature to decrease by as much as 11°C in six hours (Mortimer 1975). The scale of the offshore distance over which this upwelling takes place depends on the wind stress and nearshore bathymetry, and is typically on the order of 5–10 km. An example of extreme upwelling of colder water that covered the eastern third of Lake Michigan after three days of northerly winds is given by Ayers et al. (1958, p. 68, Fig. 27).

The balance of forces in the region of upwelling is between the wind stress, Coriolis force, and internal pressure gradient. When the wind subsides, a new balance of forces must be established. If the bottom is flat, this results in two types of free internal waves: the Poincaré wave and the Kelvin wave. As discussed by Schwab (1977), Poincaré waves are a basinwide response with oscillations in the thermocline across the entire lake. The lowest order Poincaré wave has maximum wave amplitudes on opposite sides of the lake, with a node at the center. Poincaré waves are characterized by anticyclonic phase progression, and their period is slightly less than the inertial period, which is near 17.5 h for central Lake Michigan.

The internal Kelvin wave is a coastally trapped response of the thermocline that progresses cyclonically around the lake. The Rossby deformation radius is the  $e$ -folding scale for the amplitude of this wave as a function of distance from shore. For midlatitude lakes, the baroclinic Rossby radius is typically 3–5 km. The Kelvin wave period is generally much greater than the inertial period. Schwab (1977) calculated the internal free modes of oscillation in a two-layer model of Lake Ontario assuming uniform equivalent depth. The lowest frequency mode was an internal Kelvin wave with a period of 25 days.

For lakes with sloping bathymetry, another important free wave response should be added—the topographic wave. Unlike the Poincaré and Kelvin waves, the topographic wave is a vorticity wave that can exist only in the presence of both depth gradients and the earth's rotation (Saylor et al. 1980). It is a barotropic response and is relatively insensitive to stratification.

It has been observed that when strong wind events cease, the region of upwelling progresses cyclonically

around the lake at the speed of an internal Kelvin wave, either in the form of the internal Kelvin wave or as a thermal front. This was first observed by temperature observations at municipal water intakes for cities around Lake Michigan (Mortimer 1963). Later, Kelvin waves and thermal fronts were found in other large lakes: Lake Ontario (Csanady and Scott 1974; Csanady 1977; Simons and Schertzer 1987) and Lake Onega (Beletsky et al. 1994). Some indications of upwelling and thermal front progression have also been observed in satellite infrared imagery of lake surfaces (Csanady 1977; Mortimer 1988; Bolgrien and Brooks 1992).

Because Kelvin waves play an important role in large lake hydrodynamics during periods of stratification, it is essential that three-dimensional models be able to reproduce them in seasonal simulations. Therefore, in this article we will examine wind-induced upwelling in an idealized circular basin and in Lake Michigan, and the subsequent progression of the upwelled water around the lake. Earlier experience (Bennett 1977; Beletsky et al. 1994) showed that three-dimensional models have simulated upwelling, but have not accurately duplicated the subsequent Kelvin wave progression around the lake. This is generally because of high dissipation in numerical models, whereas in real lakes friction has a relatively smaller effect. It is also necessary to have a high enough grid resolution to resolve the dynamics of nearshore barotropic and baroclinic processes (Bennett 1977). In particular, Bennett and Campbell (1987) found that a major source of numerical error for barotropic problems was the approximation of the coastline and bottom topography by the finite-difference grid. They concluded that the grid resolution had to be at least 5 km to adequately represent topographic modes in large lakes. To model baroclinic coastal currents, in particular coastal jets, the numerical grid resolution should be at least comparable to the baroclinic Rossby deformation radius.

Two three-dimensional primitive equation numerical ocean models developed specifically for the coastal ocean, the Princeton model (sometimes called POM or Princeton Ocean Model) described by Blumberg and Mellor (1987) and the Dietrich/Center for Air Sea Technology (DIECAST) model described by Dietrich and Ko (1994) will be used here. The DIECAST model with a  $z$ -level vertical coordinate and Arakawa A-grid has been successfully applied to model large lakes, as was demonstrated by Zuur and Dietrich (1990) for Lake Neuchâtel. The POM with a terrain-following (sigma) vertical coordinate and Arakawa C-grid has been used to model both wind-forced water level fluctuations and upwelling events in Lake Erie (O'Connor and Schwab 1994). This model is presently being used operationally with forecasting systems developed for the Great Lakes (Schwab and Bedford 1994), the U.S. East Coast (Aikman et al. 1996), and the Straits of Florida (Mooers and Wang 1996).

To compare model performance in the coastal envi-

ronment, it will be useful to study model responses for the basic case of upwelling and Kelvin wave propagation with idealized wind forcing and simple topographies. Moreover, unlike the real-world simulation where several factors can influence coastal hydrodynamics simultaneously, here we can isolate the influence of topographic effects or the wind forcing. Having two models can be particularly important in the cases with strong nonlinearity, when no analytical solution is available. In this case, similarity in model responses increases our confidence in model performance.

In this study we will also keep in mind practical considerations, evaluating the models from the point of view of their applicability either to short-term simulations in nowcast-forecast systems, or long-term simulations for the Great Lakes. Therefore, we are not proposing any rigorous test of finite difference schemes, or any detailed comparison with analytic solutions. Rather, we will examine how well these models can represent upwelling and internal Kelvin waves in the Great Lakes. The accurate, low dissipation modeling of upwelling, Kelvin waves, and propagating thermal fronts would be a significant achievement for a numerical model.

The outline of this paper is as follows: In section 2, we discuss the two numerical models. In section 3, we discuss the circular lake test domain, model parameters, and wind forcing, and make the model comparison tests. The models are applied to Lake Michigan in section 4, and in section 5 the results are discussed.

## 2. Model descriptions

We will investigate the response of a thermally stratified lake to wind forcing with two numerical ocean circulation models, the Princeton model and the DIECAST model. Both are nonlinear, fully three-dimensional, primitive equation, finite difference models that solve the Navier–Stokes equations of fluid dynamics. In order to discuss the common physics, we present the dynamical equations in Cartesian coordinates. The velocity components ( $u, v, w$ ) are in the ( $x, y, z$ ) directions. The mass continuity equation is

$$\nabla \cdot \mathbf{V} + \frac{\partial w}{\partial z} = 0,$$

where  $\nabla$  is the horizontal gradient operator, and  $\mathbf{V} = (u, v)$  is the horizontal velocity. The horizontal momentum equations are

$$\begin{aligned} \frac{\partial u}{\partial t} + \mathbf{V} \cdot \nabla u + w \frac{\partial u}{\partial z} \\ = -\frac{1}{\rho_o} \frac{\partial p}{\partial x} + fv + \frac{\partial}{\partial x} \left( A_m \frac{\partial u}{\partial x} \right) + \frac{\partial}{\partial y} \left( A_m \frac{\partial u}{\partial y} \right) \\ + \frac{\partial}{\partial z} \left( K_m \frac{\partial u}{\partial z} \right) \end{aligned}$$

$$\begin{aligned} \frac{\partial v}{\partial t} + \mathbf{V} \cdot \nabla v + w \frac{\partial v}{\partial z} \\ = -\frac{1}{\rho_o} \frac{\partial p}{\partial y} - fu + \frac{\partial}{\partial x} \left( A_m \frac{\partial v}{\partial x} \right) + \frac{\partial}{\partial y} \left( A_m \frac{\partial v}{\partial y} \right) \\ + \frac{\partial}{\partial z} \left( K_m \frac{\partial v}{\partial z} \right), \end{aligned}$$

where  $\rho$  is density,  $p$  is pressure,  $f$  is the Coriolis parameter, and  $A_m$  and  $K_m$  are the horizontal and vertical momentum eddy viscosities, respectively. The Eulerian derivatives at a point are the result of the horizontal and vertical velocity advections, horizontal pressure gradient force, Coriolis force, and horizontal and vertical momentum diffusion. The models are hydrostatic and Boussinesq so that density variations are neglected except where they are multiplied by gravity in the buoyancy force. The internal energy conservation equation with no sources or sinks of heat gives an expression for the temperature  $T$

$$\begin{aligned} \frac{\partial T}{\partial t} + \mathbf{V} \cdot \nabla T + w \frac{\partial T}{\partial z} \\ = \frac{\partial}{\partial x} \left( A_h \frac{\partial T}{\partial x} \right) + \frac{\partial}{\partial y} \left( A_h \frac{\partial T}{\partial y} \right) + \frac{\partial}{\partial z} \left( K_h \frac{\partial T}{\partial z} \right), \end{aligned}$$

where  $A_h$  and  $K_h$  are the horizontal and vertical thermal diffusivities, respectively. Both models use wind stress forcing at the surface, zero heat flux at the surface and bottom, free-slip lateral boundary conditions, and quadratic bottom friction. Each model uses its own parameterization of vertical and horizontal turbulent mixing, and its own finite differencing scheme, so we will give a more detailed description of each separately.

### a. Princeton model

The finite difference form of the Princeton model is described by Blumberg and Mellor (1987). Horizontal diffusion is calculated with a Smagorinsky eddy parameterization (with a multiplier of 0.1) to give a greater mixing coefficient near strong horizontal gradients. Horizontal momentum diffusion is assumed to be equal to horizontal thermal diffusion. The equation of state (Mellor 1991) calculates the density as a function of temperature, salinity, and pressure. For applications to the Great Lakes, the salinity is set to a constant value of 0.2 psu. The equations are written in terrain-following ( $\sigma = z/h$ , where  $h$  is depth) coordinates in the vertical, and in tensor form for generalized orthogonal curvilinear coordinates in the horizontal. The equations are written in flux form, and the finite differencing is done on an Arakawa C-grid using a control volume formalism. The finite differencing scheme is second order and centered in space and time (leapfrog).

A stratified body of water such as a lake has two

types of motions, the barotropic (density independent) mode and the baroclinic (density dependent) mode. The POM uses a mode-splitting technique that solves the barotropic mode for the free surface and vertically averaged horizontal currents, and the baroclinic mode for the fully three-dimensional temperature, turbulence, and current structure. This technique necessitates specifying both a barotropic and baroclinic mode time step in accordance with the Courant–Friedrich–Lewy computational stability criterion.

The model includes the Mellor and Yamada (1982) level 2.5 turbulence closure parameterization. The vertical mixing coefficients for momentum  $K_m$  and heat  $K_h$  are calculated from the variables describing the flow regime. The turbulence field is described by prognostic equations for the turbulent kinetic energy  $q^2/2$  and turbulent length scale  $l$ ,

$$\begin{aligned} \frac{\partial q^2}{\partial t} + \mathbf{V} \cdot \nabla q^2 + w \frac{\partial q^2}{\partial z} &= \frac{\partial}{\partial z} \left[ K_q \frac{\partial q^2}{\partial z} \right] + 2K_m \left[ \left( \frac{\partial u}{\partial z} \right)^2 + \left( \frac{\partial v}{\partial z} \right)^2 \right] \\ &+ 2K_h \frac{g}{\rho_o} \frac{\partial \rho}{\partial z} - \frac{2q^3}{B_1 l} \\ \frac{\partial(q^2 l)}{\partial t} + \mathbf{V} \cdot \nabla(q^2 l) + w \frac{\partial(q^2 l)}{\partial z} &= \frac{\partial}{\partial z} \left[ K_q \frac{\partial(q^2 l)}{\partial z} \right] + l E_1 K_m \left[ \left( \frac{\partial u}{\partial z} \right)^2 + \left( \frac{\partial v}{\partial z} \right)^2 \right] \\ &+ l E_1 K_h \frac{g}{\rho_o} \frac{\partial \rho}{\partial z} - \frac{q^3}{B_1} \tilde{W}. \end{aligned}$$

The first term on the right in each equation arises from the vertical diffusion of turbulent kinetic energy, and  $K_q$  is the diffusivity for this variable. The next two terms arise from the production of turbulent kinetic energy from shear and from buoyancy, respectively. The last terms with  $q^3$  represent the dissipation of turbulent energy. The  $B_1$  and  $E_1$  are empirical constants,  $g$  is the acceleration of gravity, and  $\tilde{W}$  is an empirical wall proximity function, which approaches unity away from the surface. The problem is closed by expressing the vertical mixing coefficients for momentum, heat, and turbulent kinetic energy in the form

$$\begin{aligned} K_m &= l q S_m \\ K_h &= l q S_h \\ K_q &= l q S_q, \end{aligned}$$

where  $S_m$ ,  $S_h$ , and  $S_q$  are analytically derived algebraic stability functions. Details of this procedure are given by Blumberg and Mellor (1987).

### b. DIECAST model

The DIECAST model is described by Dietrich et al. (1990) and Dietrich (1993). It is designed as a free-stream model that describes the flow regime in a water body using a simple nonlinear bottom drag. The grid points are at constant  $z$ -level depths. The finite difference equations are written for the Arakawa A-grid, using a filtered leapfrog trapezoidal scheme that is centered in space and time. Incompressibility is satisfied by constructing a three-dimensionally nondivergent advection velocity at the standard Arakawa C-grid locations. A fourth-order approximation is used for the baroclinic pressure gradient, giving good accuracy for adequately resolved features. The Coriolis and vertical diffusion terms are coupled with an implicit treatment so that the Coriolis terms conserve energy exactly in the algebraic sense. This finite differencing scheme results in a low dissipation model with a computationally efficient code. The low dissipation of the model makes it particularly well suited to modeling smaller-scale nonlinear processes such as eddy shedding, fronts, and frontal eddies, which occur in the Gulf of Mexico Loop Current (Dietrich and Ko 1994; Dietrich and Lin 1994).

The equation of state computes the density as a quadratic function of temperature only (Simons 1973). The bottom drag coefficient is set to the constant value 0.002. The model uses a rigid-lid approximation. This filters out free surface waves, which interact little with the general flow except in problems where the barotropic seiche is important. The surface pressure (against the lid) is equivalent to a hydrostatic pressure head (i.e., surface elevation anomaly) and is determined by a Poisson equation. To solve this equation the domain is rectangularized by a “swamp layer” approximation, which leads to creeping flow over land [typically less than  $1 \text{ mm s}^{-1}$  after a short initial transient of  $O(1) \text{ cm s}^{-1}$ ]. This creeping flow can be entirely eliminated by using a rapidly converging iteration (Dietrich and Ko 1994).

Since the model runs with low dissipation even for arbitrarily steep topography, it is not necessary to use physically artificial eddy diffusivities for numerical stability purposes. The horizontal diffusivities for heat and momentum are set to the constant value  $A = 1 \text{ m}^2 \text{ s}^{-1}$ . The vertical viscosity

$$K_m = K_o + K(|\boldsymbol{\tau}|, \text{Ri})$$

is the sum of a background vertical viscosity  $K_o = 10^{-5} \text{ m}^2 \text{ s}^{-1}$ , and an empirical relation to account for wind stress  $\boldsymbol{\tau}$  (in  $\text{dyn cm}^{-2}$ ), and stratification

$$K(|\boldsymbol{\tau}|, \text{Ri}) = \frac{\alpha |\boldsymbol{\tau}|}{(1 + 10\text{Ri})^{3/2}}, \quad 5 \leq \alpha \leq 25,$$

based on the gradient Richardson number

$$\text{Ri} = \frac{g\beta T_z}{u_z^2 + v_z^2},$$

where the coefficient of thermal expansion for water is

$\beta = 2 \times 10^{-4} \text{C}^{-1}$ . The empirical constant  $\alpha$  in the numerator is adjusted for the vertical grid spacing and is smaller for increased vertical resolution. The model parameterization instantaneously mixes the epilimnion if cold water appears over warm water near the surface. The physical assumptions for using Richardson number parameterizations are discussed by McCormick and Meadows (1988). Despite its empirical nature, this type of parameterization has had success in numerous applications, including the Great Lakes (Heinrich et al. 1981; McCormick and Scavia 1981). The vertical heat diffusivity is parameterized as

$$K_h = K_o + 0.1K(|\tau|, Ri),$$

so that the wind-forced turbulent heat mixing is less than the momentum mixing. Physically, this parameterization has been used because internal waves have been observed to be more efficient at transferring momentum than heat (after a wave passes a given point, it tends to retain its original density, while pressure forces can lead to momentum exchange). Another reason is that upwelling is essentially a convective flow regime, and cannot be simulated realistically if model diffusion is the dominant process. In particular, after a strong wind event, the vertical diffusion reverts to the very small background value  $K_o$ , allowing subsequent free wave propagation to be modeled with low dissipation.

### 3. Circular lake tests

In order to determine how well the models simulate internal Kelvin waves resulting from wind-induced upwelling and subsequent relaxation of the thermocline, the free wave responses to representative wind forcing will be examined for various grid resolutions and bathymetries. Both models will be started from the same initial temperature distribution and forced with the same wind stress. We will use a circular basin the size of a moderately large lake, with a diameter of 100 km, centered at latitude  $42^\circ\text{N}$ , so that the Coriolis parameter varies slightly but is near  $f = 10^{-4} \text{s}^{-1}$ . The models will be tested on a simple rectangular Cartesian grid with  $\Delta x = \Delta y$ . Grid spacings of 5 km ( $22 \times 22$  points), 2.5 km ( $42 \times 42$  points), and 1.25 km ( $82 \times 82$  points) are used in order to investigate the sensitivity of the model results to grid resolution. The lake diameter is always 100 km. Two bottom topographies will be used: One is a basin of 100-m constant depth, and the other is a basin with a parabolic depth profile of maximum depth 100 m. To insure computational stability, the DIECAST model uses a time step of 600 s for the 5-km and 2.5-km grids, and 300 s for the 1.25-km grid. The POM uses internal mode time steps of 1200, 600, and 300 s, and external mode time steps of 40, 20, and 10 s for the 5-km, 2.5-km, and 1.25-km grids, respectively. The vertical resolution in the model depends on the case being studied.

Since our desire is to study the effect of wind forcing

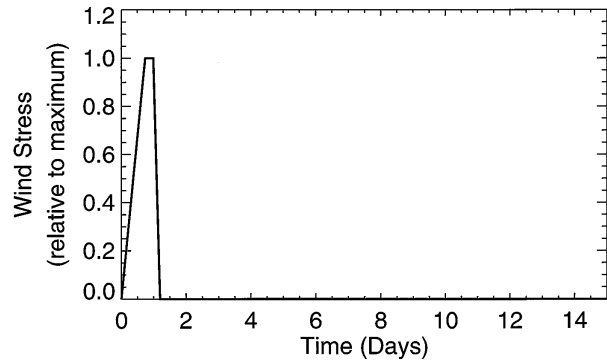


FIG. 1. Time variation of wind stress forcing.

on a stratified lake, we will use stratified conditions commonly observed in the Great Lakes during summer and early fall. The cases we study will be initialized with the epilimnion above 5 m isothermal at  $20^\circ\text{C}$ , the hypolimnion below 15 m isothermal at  $5^\circ\text{C}$ , and a linear temperature decrease across the thermocline. This sharp thermocline will concentrate the energy of the response primarily in the first vertical mode. No heat flux is applied during the simulations. The surface heat flux becomes important only on longer time scales than are considered in this paper, namely from monthly to seasonal. Since we do not include surface heat flux, the differences in the vertical turbulent thermal mixing parameterization between the models will not have a significant effect.

A spatially uniform wind stress is used in order to generate primarily the lowest horizontal mode Kelvin wave. The wind forcing we use is representative of short duration wind storms that impart momentum impulsively to the Great Lakes, resulting in a nearly free internal wave response. The wind stress increases linearly from zero to its maximum value ( $0.01$  or  $0.3 \text{ N m}^{-2}$ ) over 18 hours, approximately one inertial period for this latitude. The wind stress remains constant at this maximum value for another 6 hours, until time 1 day, and then decreases linearly to zero during the next 5 hours. The wind forcing then remains at zero for the duration of the model simulation (Fig. 1). Typically, the conditions in the Great Lakes at any given time are most strongly influenced by the most recent wind forcing. However, in some cases, coastally trapped waves can propagate for up to 20 days (Bennett and Lindstrom 1977; Boyce et al. 1989), or longer (Saylor et al. 1980). Therefore, the simulation time should be comparable to the time of maximum effective memory of large lakes. In our study it was chosen to be 15 days.

#### a. Kelvin wave over flat bottom

First, we will study the internal Kelvin wave. Although the model equations include nonlinear terms, we will minimize their effect by generating a Kelvin wave of small amplitude. The lake bathymetry will be a con-

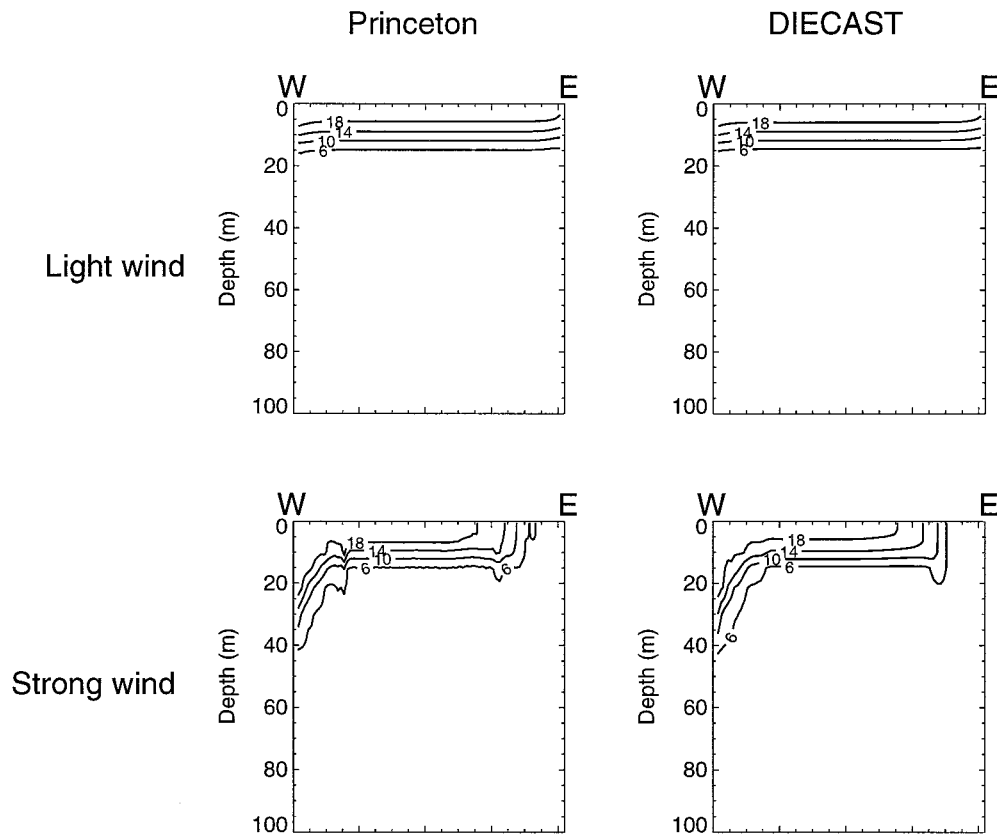


FIG. 2. East-west cross section of temperature distribution at the moment of maximum upwelling development (day 1.2) in the circular flat-bottom basin tests.

stant depth of 100 m. This allows the Kelvin wave response to be isolated from the effects of bottom topography. This problem has been studied analytically by Csanady (1968; 1984), and for a three-layer system described above the speed of the linear inviscid internal Kelvin wave (first baroclinic mode) is  $c = 0.36 \text{ m s}^{-1}$ . Note that this wave speed can be substantially reduced because of physical and numerical diffusion (Davey et al. 1983; Hsieh et al. 1983).

The linear Kelvin wave is best represented by a weak upwelling event where the thermocline does not become too steep and break the surface, since the strong upwelling phenomenon requires nonlinear dynamics for its description. A vertical cross section of the temperature field at the time of maximum thermocline displacement for the 1.25-km grid case is shown in the upper panel of Fig. 2. (All illustrations in Figs. 2–12 correspond to results from the highest resolution 1.25-km grid cases.) The northerly wind forcing results in upwelling along the eastern side and downwelling along the western side of the basin. The wind stress forcing of  $10^{-2} \text{ N m}^{-2}$ , corresponding to a wind speed of approximately  $3 \text{ m s}^{-1}$ , yields a weak upwelling that does not break the surface. When the wind subsides, the subsequent dynamical response is the cyclonic progression of the upwelling and downwelling regions around

the basin. We shall examine this Kelvin wave response at the center of the thermocline. The Rossby deformation radius is  $r = c/f$ . For the values given above we have  $r = 4 \text{ km}$ , so that the model grid spacings are on the order of the Rossby radius or less. Since the basin depth is constant, the nondimensional  $\sigma$  levels correspond to  $z$ -level depths. For this case both models were run with 13 vertical levels. Model runs with more vertical levels (not shown) produced essentially the same results. The Princeton model has grid levels at  $\sigma = 0, -0.01, -0.02, -0.03, -0.05, -0.08, -0.12, -0.18, -0.25, -0.35, -0.50, -0.70, \text{ and } -1.0$ . The DIECAST model has the same 13 constant depth levels at  $z = 0, 1, 2, 3, 5, 8, 12, 18, 25, 35, 50, 70, \text{ and } 100 \text{ m}$ .

For the POM and DIECAST model, horizontal cross-sectional plots at the 10-m level were made for both temperature and current fields. The boundary of the sinking warm water is associated with the  $13^\circ\text{C}$  isotherm, and the boundary of the rising cold water is associated with the  $12^\circ\text{C}$  isotherm (Fig. 3). The wave motion is evident from the progression of these warm and cold regions shown by the isotherms, and the two stagnation point nodes in the azimuthal velocity field along the shore (not shown), which separate regions of upwelling and downwelling.

We measured the wave speed by plotting a time series

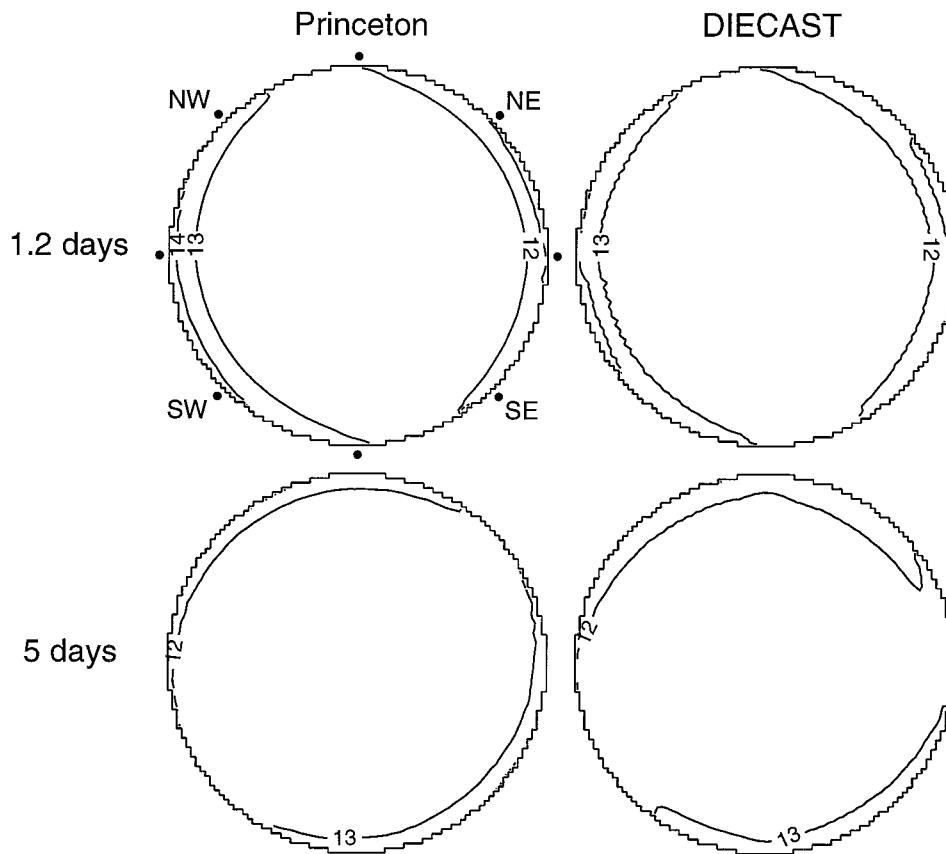


FIG. 3. Temperature at 10-m depth for the Kelvin wave case: flat-bottom basin, light northerly wind, at days 1.2 and 5.

of the temperature and velocity components at 10-m depth at eight equally spaced grid points around the basin (as indicated by the dots around the circumference of the upper left plot in Fig. 3). The time series of temperature (Fig. 4) did not show any steepening of the warm front as can occur for nonlinear Kelvin waves (Bennett 1973), probably because we have minimized this effect by choosing a wave of small amplitude. The wave speed was calculated by tracing the propagation of the temperature maximum and minimum, and the two velocity nodes around the basin, and then averaging. These four methods of calculating wave speeds give closer results with increasing grid resolution. Results of these calculations are shown in Table 1. Both models appear to be approaching grid convergence.

The wave speed increases with increasing grid resolution, although not dramatically in the Princeton model. DIECAST results are more sensitive to horizontal resolution. The wave speed is slightly higher in the POM compared to the DIECAST: 0.24 versus 0.22  $\text{m s}^{-1}$  in the fine resolution (1.25 km) grid case, which is about 65% of the inviscid analytic solution. This is probably because of insufficient horizontal resolution for the given internal Rossby radius. With a Rossby radius of 4 km, the Kelvin wave scale is only marginally resolved.

In addition, certain aspects of the DIECAST model could result in a lower Kelvin wave speed and also damp higher frequency modes such as Poincaré waves. They are not inherent features of its formulation, but rather were chosen for efficient modeling of slower modes that dominate lake and ocean general circulation. These are a moderate time filter designed to selectively damp the fast modes (which are often noise because of poor initial values) and fully (backward) implicit Coriolis terms. A new version of the DIECAST model will improve some of these aspects (Dietrich 1996). Reducing the explicit horizontal momentum and heat diffusivities by an order of magnitude, and even to zero in both models, did not increase the Kelvin wave speed, although more noise was produced.

#### b. Full upwelling over flat bottom

The full upwelling case is examined using the same time variation of the wind as for the linear case, but with a maximum wind stress of  $0.3 \text{ N m}^{-2}$ , corresponding to a wind speed of  $12 \text{ m s}^{-1}$ . This forcing results in upwelling that breaks the surface (Fig. 2). One can even see an indication of an internal bore developing in the downwelling area (POM results), which is about

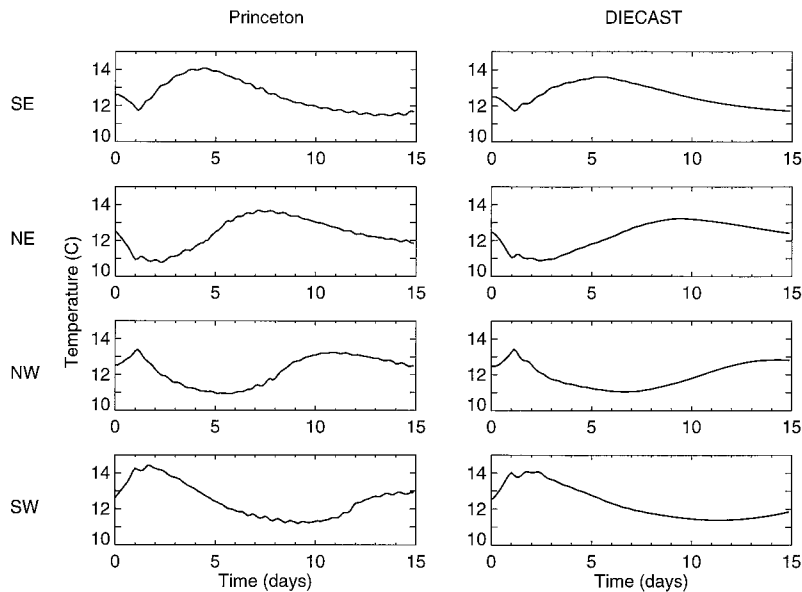


FIG. 4. Time series of temperature at 10-m depth at four points along the coast in the Kelvin wave case, flat-bottom basin.

to start its propagation offshore. This is a short-term phenomenon though, and it is not important in this study. The models are again run to 15 days, and both give qualitatively similar full upwelling and relaxation patterns. The most pronounced coastal zone features plotted on a horizontal cross section at 10 m (Fig. 5) are the warm and cold fronts advancing along the coast and cutting off cold and warm lenses, respectively, in the interior. Interestingly, a somewhat similar evolution of the temperature pattern was found by Wajsowicz and Gill (1986) for the early stages of adjustment in the ocean due to coastal Kelvin wave propagation. This similarity is explained by the fact that during the early stage of adjustment in the ocean we can ignore planetary wave propagation and  $\beta$  dynamics.

The azimuthal velocity nodes are again at the frontal boundaries. The warm front is marked by steep temperature and velocity increases on the time series plots (Fig. 6), with inertial oscillations in the velocity before its passage. The warm front stays relatively sharp, although the temperature difference across the front decreases from 15° to 5°C. In contrast, the cold front diffuses rapidly after the wind cessation and then remains relatively weak. Poincaré waves are pronounced offshore, especially in the Princeton model. The wave

speeds were calculated by tracking the progression of the warm and cold fronts that rotate cyclonically around the lake. Like in the Kelvin wave case, the speed was fastest for the highest resolution (Table 2), and the POM exhibits higher speeds than the DIECAST model. While DIECAST shows essentially the same wave speed in the Kelvin wave and full upwelling cases, the POM is more sensitive to horizontal resolution in the full upwelling case.

### c. Kelvin wave over parabolic bathymetry

Next, the effects of variable bottom topography will be studied for the same circular basin with a parabolic depth profile (Fig. 7). We shall first examine the upwelling response to a weak wind forcing of  $10^{-2} \text{ N m}^{-2}$  with the same impulsive time distribution as in the previous cases. An exact comparison between a  $\sigma$ -level and  $z$ -level model can be made only for a domain of constant depth. For the same number of levels, the  $\sigma$ -coordinate model will have the levels closer together in the shallower regions over sloping topography and give more resolution to the temperature gradient in the thermocline there. Furthermore, over sloping bathymetry, the horizontal pressure gradient in  $\sigma$  coordinates is calculated as the sum of two nearly equal but oppositely signed terms and the hydrostatic consistency criterion given by Haney (1991)

$$\left| \frac{\sigma}{\Delta\sigma} \frac{\Delta H}{H} \right| < 1,$$

where  $H$  is the depth, becomes a consideration. Basically, the vertical rise of a  $\sigma$  surface between two hor-

TABLE 1. Calculated Kelvin wave speeds ( $\text{m s}^{-1}$ ) for flat-bottom circular basins with light wind stress forcing ( $10^{-2} \text{ N m}^{-2}$ ).

Grid spacing (km)	POM	DIECAST
5	0.22	0.14
2.5	0.23	0.18
1.25	0.24	0.22

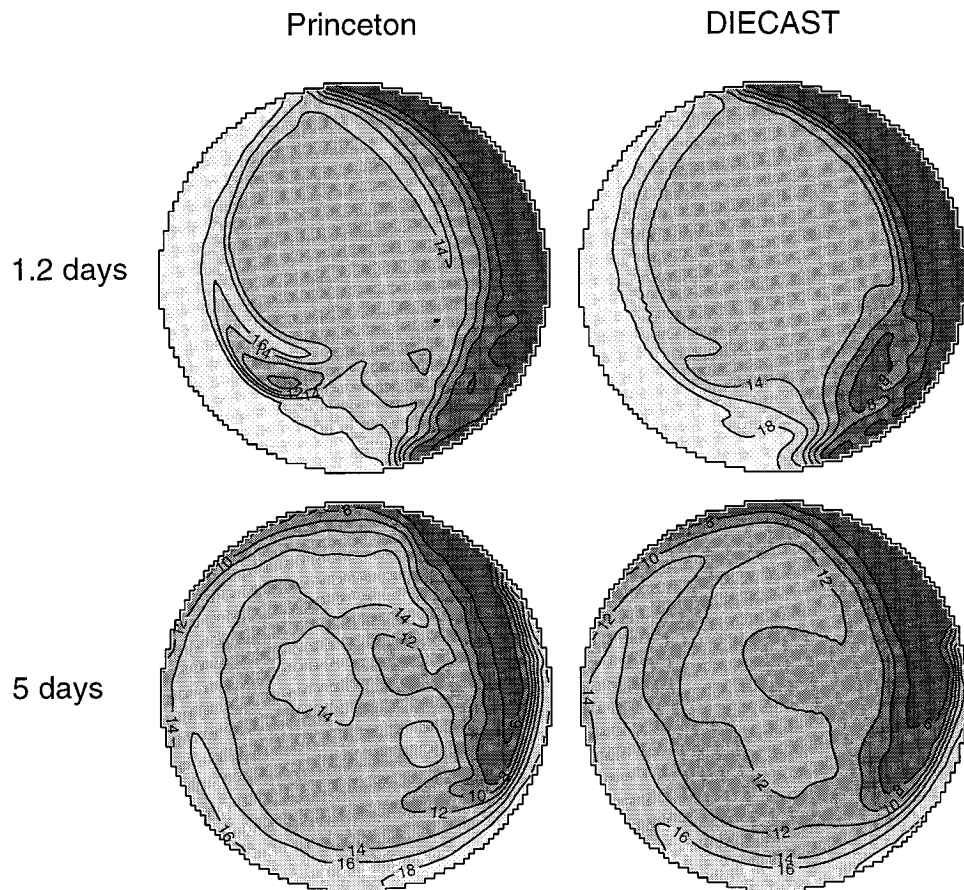


FIG. 5. Temperature at 10-m depth for the full upwelling case: flat-bottom basin, strong northerly wind, at days 1.2 and 5.

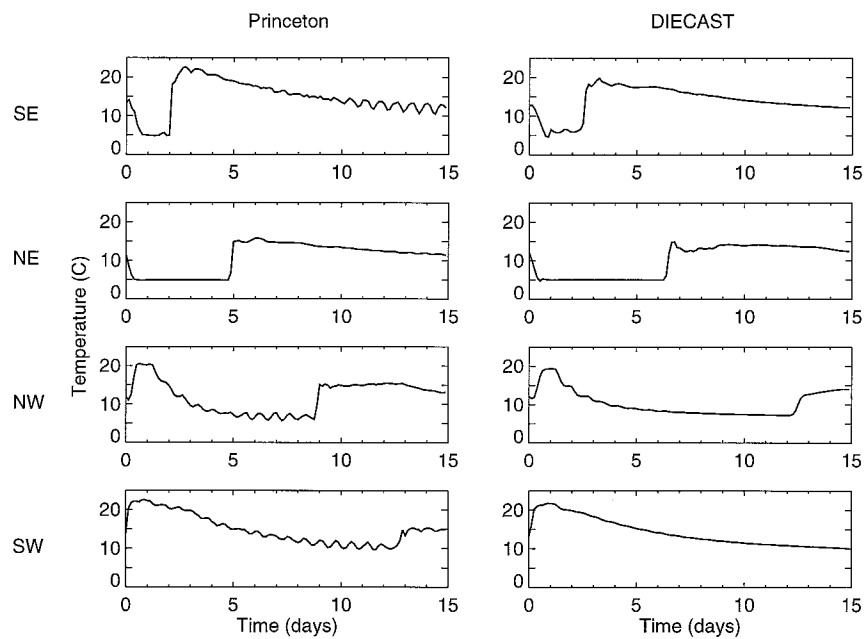


FIG. 6. Time series of temperature at 10-m depth at four points along the coast in the strong wind case, flat-bottom basin tests.

TABLE 2. Calculated frontal speeds ( $\text{m s}^{-1}$ ) for flat-bottom circular basins with strong wind forcing ( $0.3 \text{ N m}^{-2}$ ).

Grid spacing (km)	POM	DIECAST
5	0.16	0.13
2.5	0.21	0.17
1.25	0.28	0.20

horizontal grid points must remain less than the vertical distance between that  $\sigma$  surface and the one immediately above. For the lake basins being considered, the bathymetry strongly influences the free modes of oscillation for the barotropic mode and the first baroclinic mode. Any  $z$ -level model must have adequate vertical resolution to represent the shape of the basin including the deepest regions, and any  $\sigma$ -level model must have adequate vertical resolution to calculate the horizontal pressure gradient even in the steepest regions. The maximum depth of the parabolic basin is always 100 m, but the depths at the shore depend on the grid. To adequately resolve the upwelling over a sloping bottom, the vertical grid resolution in the  $z$ -level model was increased, so the DIECAST model was run with 29 levels, at depths 0, 1, 2, 3, 4, 5, 6, 7, 8, 9, 10, 11, 12, 13, 14, 15, 16, 17, 18, 20, 25, 30, 40, 50, 60, 70, 80, 90, and 100 m. The Princeton model runs with 29 levels did not change results. Therefore, the same 13  $\sigma$ -levels as in the flat-bottom cases were used.

The Kelvin wave dynamics are significantly different

from the flat-bottom case as seen in Figs. 8 and 9. The primary effects are the generation of a topographic wave response and higher dissipation in the nearshore areas. In particular, since the initial upwelling was weak, we were only able to trace the Kelvin wave propagation in the 1.25-km and 2.5-km grid cases. The temperature diffuses too quickly in the 5-km grid case. Another effect that masks Kelvin wave propagation, especially in the Princeton model, is an adjustment of the temperature field to boundary conditions: The bottom boundary condition of zero heat flux causes the isotherms to curve downward and intersect the sloping bottom orthogonally. As Schwab et al. (1995) showed, in the absence of wind, this boundary condition will cause a dome-shaped thermocline. Since the wind impulse was weak enough in our case, we can see the development of the temperature adjustment process in Fig. 8, which masks the Kelvin wave propagation clearly seen in the time series of temperature (Fig. 9). The speed of the Kelvin wave was higher in the Princeton model than in DIECAST (Table 3). The speed increases with greater resolution as in the flat-bottom case, but is always higher than in the flat-bottom case, probably because of the interaction with the topographic wave.

*d. Full upwelling over parabolic bathymetry*

The same strong wind forcing of  $0.3 \text{ N m}^{-2}$  is used. Both models give qualitatively similar results (Figs. 7 and 10) with a somewhat more localized upwelling front

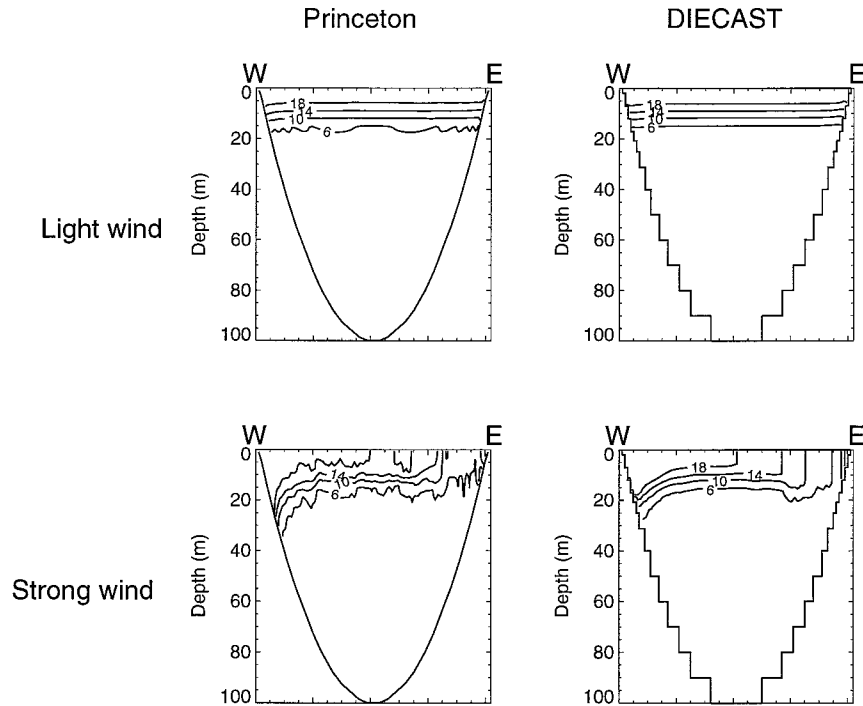


FIG. 7. East-west cross section of temperature distribution at the moment of maximum upwelling development (day 1.2) in the circular paraboloid basin tests.

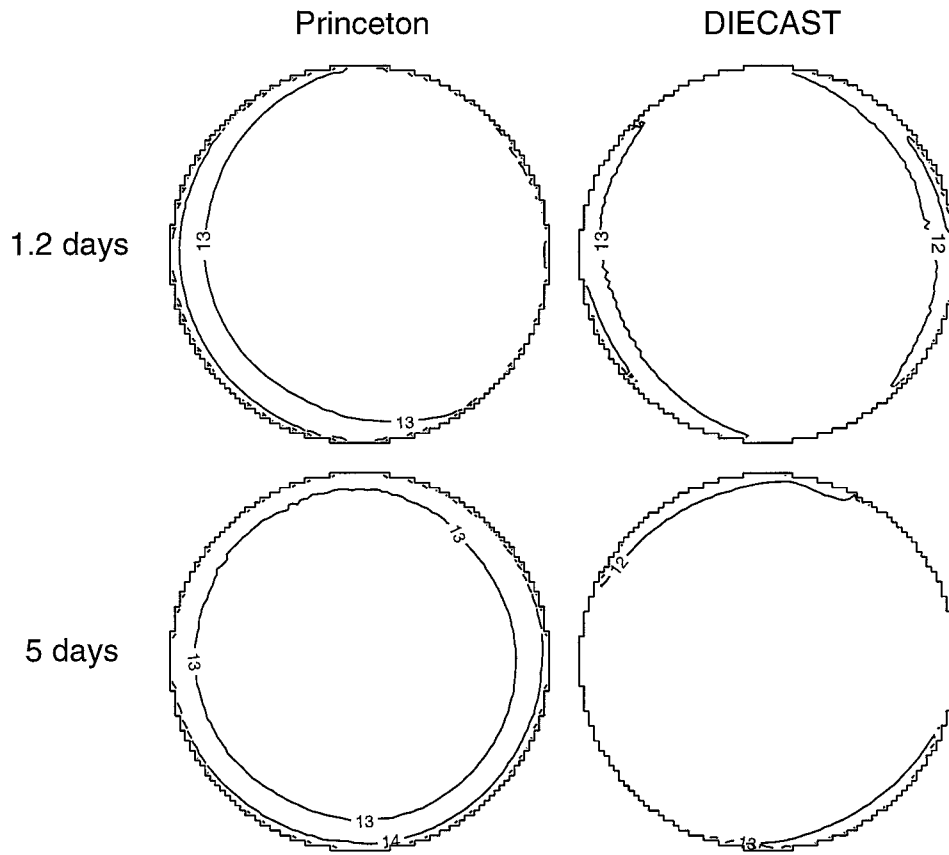


FIG. 8. Temperature at 10-m depth for the Kelvin wave case: circular paraboloid basin, light northerly wind, at days 1.2 and 5.

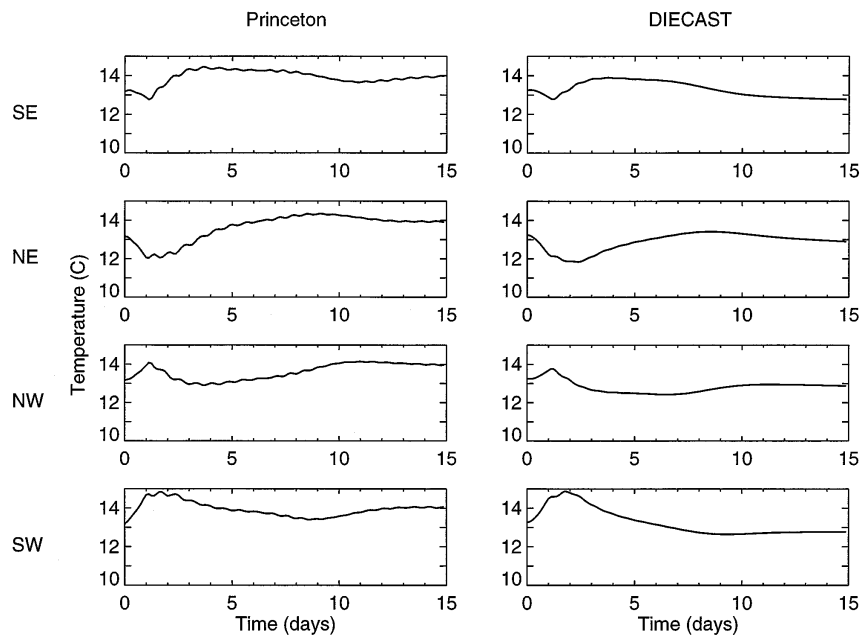


FIG. 9. Time series of temperature at 10-m depth at four points along the coast in the Kelvin wave case, circular paraboloid basin tests.

TABLE 3. Calculated Kelvin wave speeds ( $\text{m s}^{-1}$ ) for parabolic bottom circular basins with light wind forcing ( $10^{-2} \text{ N m}^{-2}$ ).

Grid spacing (km)	POM	DIECAST
2.5	0.27	0.22
1.25	0.30	0.24

and more pronounced Poincaré waves in the POM. The fronts are not as strong as in the flat-bottom case, as seen in the time series plots of temperature (Fig. 11). The warm front progresses around the eastern half of the basin, and the cold front progresses around the western half in the first 5 days (Fig. 10). Again, the frontal speed was higher in cases with higher grid resolution. In contrast to the Kelvin wave and full upwelling cases over a flat bottom, there was no persistent propagation of warm and cold fronts around the lake. In this strong upwelling case, the resulting large horizontal density gradients induce a strong geostrophic circulation over the sloping bottom. This geostrophic double gyre pattern is evident after 10 days (Fig. 12). Most probably, the strong geostrophic currents inhibit the propagation of both fronts around the lake. The velocity field is noticeably influenced by the topographic and Poincaré

wave responses. Both models also show a tendency to generate mesoscale eddies in the coastal zone on the 1.25-km grid after about 10 days of relaxation, although in different areas. The horizontal size of the eddies is about 5 km (Fig. 12), consistent with previous observations of baroclinically unstable currents, meandering upwelling fronts, and mesoscale eddy generation in large lakes (Rao and Doughty 1981; Beletsky et al. 1994).

The strongest upwelling over sloping bathymetry occurs in both models not at the shore, but offshore by a grid square or two (Fig. 7). This pattern has also been noted in previous modeling and observational studies for large lakes (Csanady 1984, pp. 163–165, 184). The mean depths of the grids at the shore for the Princeton model were 12, 12, and 4 m for the 5-km, 2.5-km, and 1.25-km grids, respectively. For the DIECAST model, the average depths at the shore were 7, 9, and 3 m for the 5-km, 2.5-km, and 1.25-km grids, respectively. Therefore, such factors as bottom and horizontal friction play a significant role, distorting the Ekman upwelling regime, especially in the fine-resolution grid cases.

We have applied two numerical ocean models to a circular basin. The models use different numerical schemes and different turbulence closure parameteri-

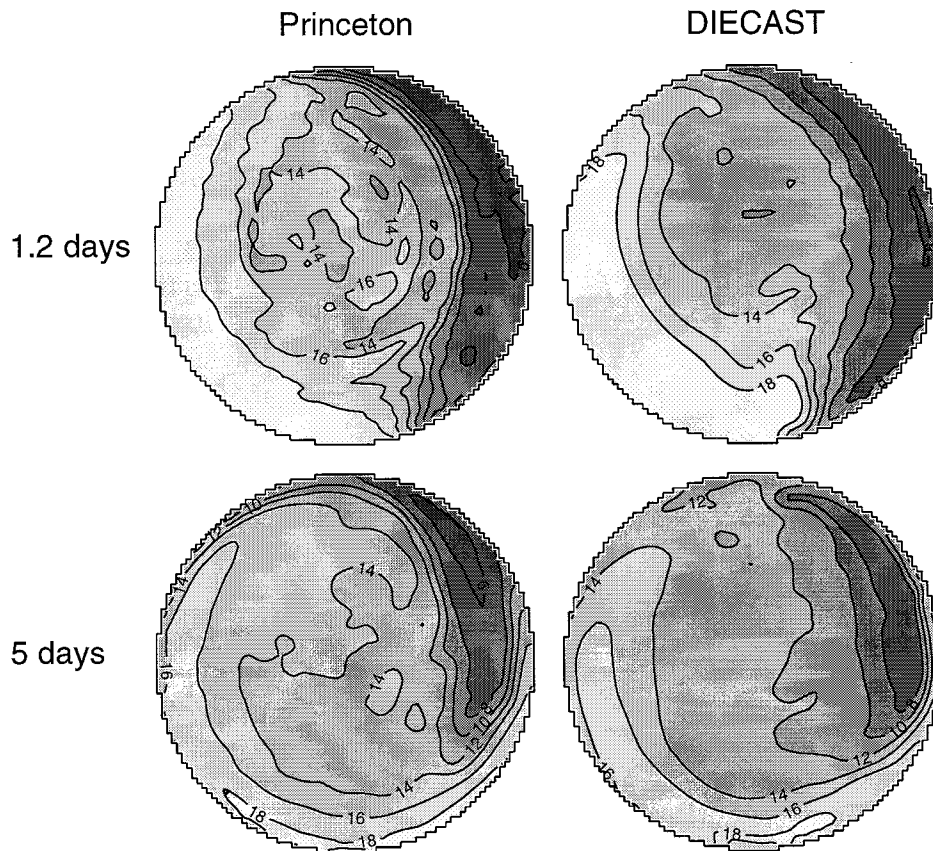


FIG. 10. Temperature at 10-m depth for the full upwelling case: circular paraboloid, strong northerly wind, at days 1.2 and 5.

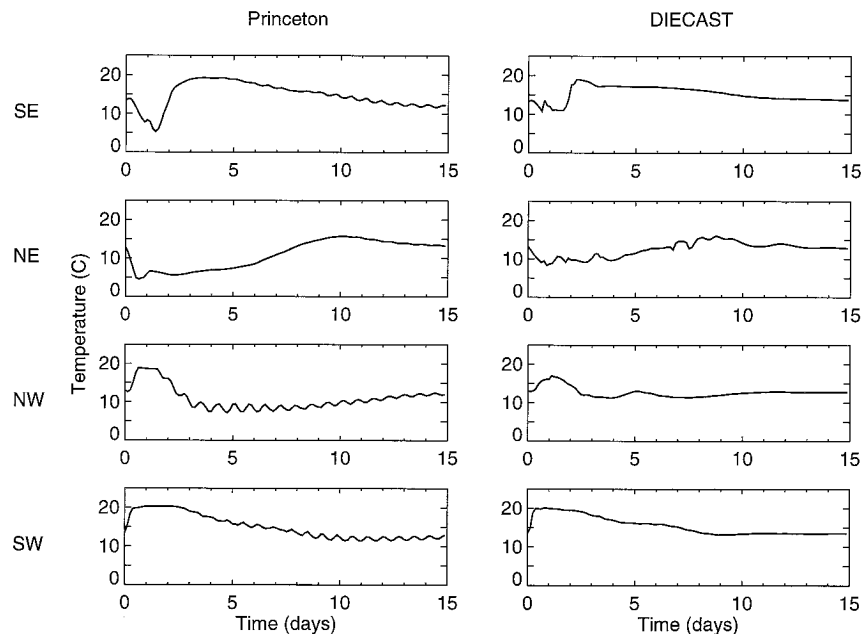


FIG. 11. Time series of temperature at 10-m depth at four points along the coast in the strong wind case for the circular paraboloid basin tests.

zations. Despite this, both models give qualitatively similar results, which encouraged us to apply the models to a strong upwelling event in Lake Michigan.

#### 4. Lake Michigan case study

Lake Michigan extends about 495 km in the north-south direction, from latitude  $41.6^{\circ}$  to  $46.1^{\circ}$ N. It is narrow compared to its length, with an average width on the order of 100 km. There are two basins, one in the southern part of maximum depth 163 m, and one in the central part with the lake's maximum depth of 262 m (Fig. 13). Here we represent the lake with a rectangular Cartesian grid with  $\Delta x = \Delta y$ . The  $x$  axis is aligned east-west, and the  $y$  axis is aligned north-south. Two grid sizes, 5 and 2 km, are used for this study. The digitized bathymetries for these domains were prepared from the Lake Michigan bathymetry described by Schwab and Sellers (1980). The bathymetries were modified so that the ratio of depths of any two adjacent grids did not exceed 0.5 in order not to exceed the hydrostatic consistency criterion for  $\sigma$ -coordinates. The 5-km grid has  $53 \times 102$  points, with a minimum depth of 2 m. The 2-km grid has  $130 \times 251$  points, with a minimum depth of 1 m. The DIECAST model uses a time step of 600 s for the 5-km grid and 300 s for the 2-km grid. The POM uses baroclinic and barotropic time steps of 900 and 30 s for the 5-km grid, and 300 and 10 s for the 2-km grid. The POM also uses the same 13  $\sigma$  levels as in the circular basin tests, but a lower horizontal eddy diffusivity multiplier (0.01 versus 0.1) was used in the 2-km case. Again, we found out that this vertical resolution was quite sufficient for the coastal upwelling

problem. The DIECAST model uses 32 vertical levels for the 5-km grid, at  $z = 0, 1, 2, 3, 4, 5, 6, 7, 8, 9, 10, 11, 12, 13, 14, 15, 16, 18, 20, 25, 30, 40, 50, 65, 80, 100, 125, 150, 175, 200, 225,$  and 262 m. Due to the larger computer memory requirement for the 2-km grid, the DIECAST model uses only 14 vertical levels, at  $z = 0, 1, 2, 3, 5, 8, 12, 16, 20, 30, 50, 100, 175,$  and 262 m.

##### a. Upwelling case description and model initialization

The case study used is one of the best known in physical limnology (Mortimer 1963). There was a strong upwelling episode along the eastern shore of Lake Michigan on 9 August 1955 resulting from strong northerly winds (Fig. 14). Before the storm, the thermocline was located between 10 and 20 m, but after 1.5 days of strong winds it had risen to the surface and shifted up to 15-km offshore, as was determined by temperature observations taken 2 days after the storm. The following week was characterized by the absence of significant wind events; thus, the thermocline relaxed with the warm front moving northward along the eastern shore. The front started at Michigan City and propagated at least to Ludington (the last point of observation available, Fig. 14). The frontal speed was about  $0.45 \text{ m s}^{-1}$ . The wind history is generally close to the wind scenario that was used previously in the circular lake studies with the maximum wind stress of  $0.3 \text{ N m}^{-2}$ . Therefore, the same wind scenario will be used in the Lake Michigan simulations.

To initialize the models one needs to know the three-dimensional thermal structure and currents in the lake.

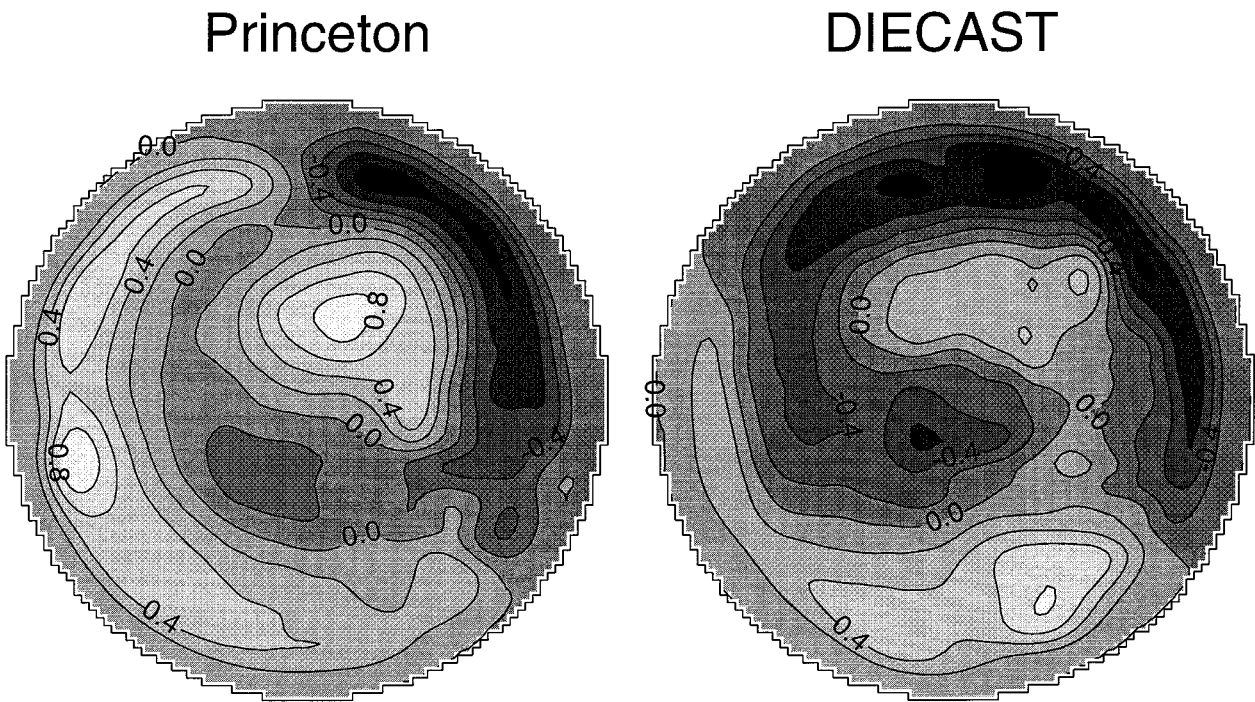


FIG. 12. Normalized streamfunction at day 10 in the circular paraboloid basin tests. Negative values indicate cyclonic vorticity, positive values anticyclonic.

To deal with this problem, we can postulate that during major wind events, wind-generated currents are usually dominant over preexisting ones. Therefore, the no-motion condition was assumed for the initial velocity field. To obtain the initial thermal structure, observations were used from several stations sampled soon after the storm, because the closest survey before the storm was made on 29 June, that is, more than a month before the upwelling episode. Only offshore stations that were outside upwelling and downwelling zones, and hence less disturbed by the storm, were used for this purpose. The critical point in the initialization is the depth of the thermocline, since it determines the wave speed in the lake. Therefore, an inverse procedure was used to obtain the initial thermocline depth assuming no horizontal temperature gradients in the lake. Using the same aforementioned wind scenario and changing initial vertical temperature profiles available from several offshore stations (Ayers et al. 1958), the models were run for 1.2 days to examine the location where the thermocline breaks the surface. The initial temperature profile that best fit the observed offshore thermocline displacement was chosen. It consists of a mixed layer 11 m deep with a temperature of 21.3°C, a strong thermocline with a 13°C temperature decrease between 11 and 15 m, and a gradual temperature decrease from 8.3°C at 15 m to 4.3°C at 100 m.

#### *b. Model results and comparison with observations*

After one day of wind forcing, both models produce strong upwelling along the east coast and downwelling

along the west coast (Fig. 15). Similar to the circular paraboloid case, the upwelling front is more localized in the POM, and the offshore temperature pattern is more complicated because of the prevalence of Poincaré waves (see Mortimer, 1963), which were much less pronounced in the DIECAST model. The models did not produce upwelling at Michigan City (cf. Fig. 14), most likely because of the idealized wind field. As the upwelling relaxes, both models show the propagation of warm and cold fronts along the east and west coasts of Lake Michigan, and both fronts cut off cold and warm lenses of water offshore (Fig. 16), as in the circular lake tests. It is also apparent from the model results that a temperature increase at a point along the coast can be the combination of warm front propagation and local downwelling. The results are qualitatively similar for the 5-km and 2-km grids, but the coastal jets, meandering upwelling fronts, and mesoscale eddies are better resolved by the 2-km grid. For both models, the propagation speed was faster for the 2-km grid.

Time series plots of temperature observations near 13-m depth at Benton Harbor, Muskegon, and Ludington, Michigan, are shown in Fig. 17 for both Princeton and DIECAST models. Since our goal is to compare model results with Mortimer's (1963) observations, only warm front results are presented. Both models give similar frontal speeds. The initially sharp thermal front gradually diffuses in both models, although in the POM it diffuses slower compared to DIECAST. There is somewhat less computational noise in the temperature

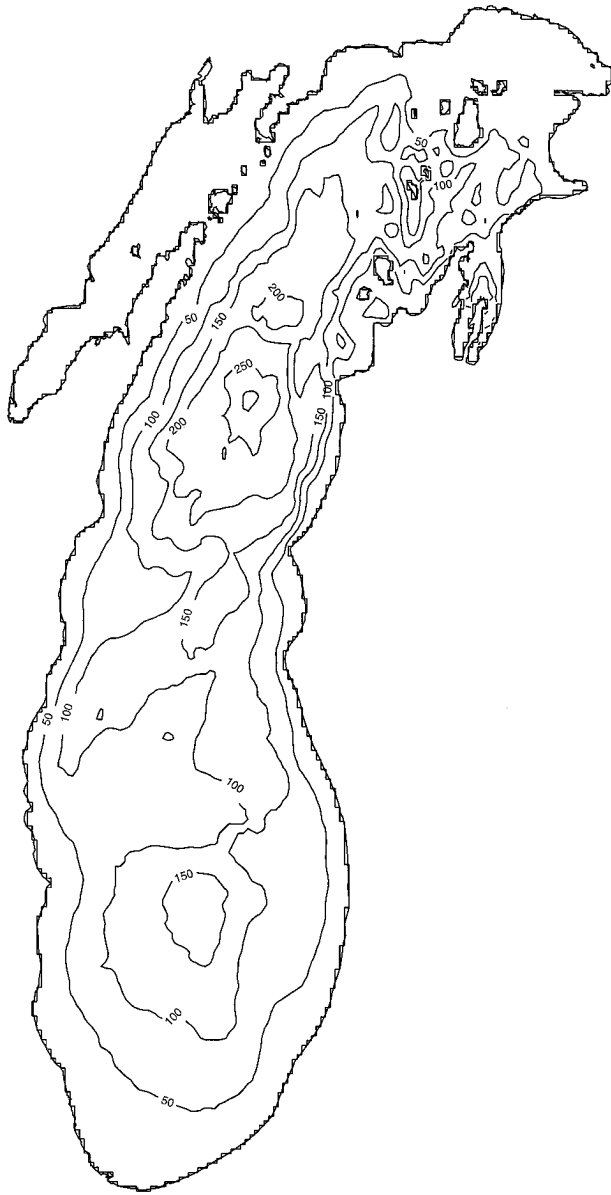


FIG. 13. Lake Michigan bathymetry, depths in meters.

field produced by the DIECAST model than in the POM results. Steepness of bottom topography is probably not that important in generation of this noise because it appears both in areas of large and small depth gradients. Because of the diffusion, the precise calculation of frontal speed is difficult, although it is obvious that both models underestimate it. An example of the speed calculation is provided by the POM in the temperature time series at Benton Harbor and Muskegon. The warm front propagation speed determined by the time between the sharp temperature increases at the 13-m depth at these two points is about  $0.28 \text{ m s}^{-1}$  compared to the observed speed of  $0.45 \text{ m s}^{-1}$ .

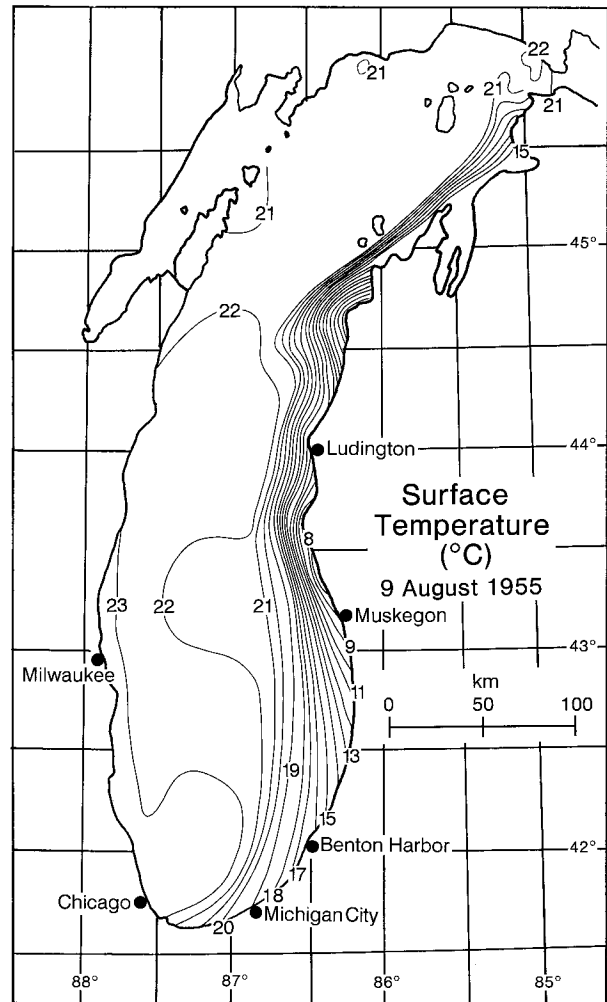


FIG. 14. Surface temperature in Lake Michigan, 9 August 1955, redrawn from Ayers (1958).

There are several possible reasons why both models underestimate the frontal speed: physical and numerical diffusion, uncertainty in the initialization of the thermal structure, and surface momentum and heat fluxes. In particular, the frontal propagation speed depends on the vertical structure of the thermocline, which may vary around the lake but was not accounted for in the model initialization. Moreover, vertical thermal structure could have changed locally during the week of Mortimer's observations because of the deepening of the thermocline due to wind-induced downwelling; surface heat flux could also have modified the vertical density gradient, although this would have a smaller influence on frontal propagation speed. In the Lake Michigan case we found again that the frontal propagation speed was not sensitive to reduction in the horizontal momentum and heat diffusivities below a certain level, although more noise was produced in both models.

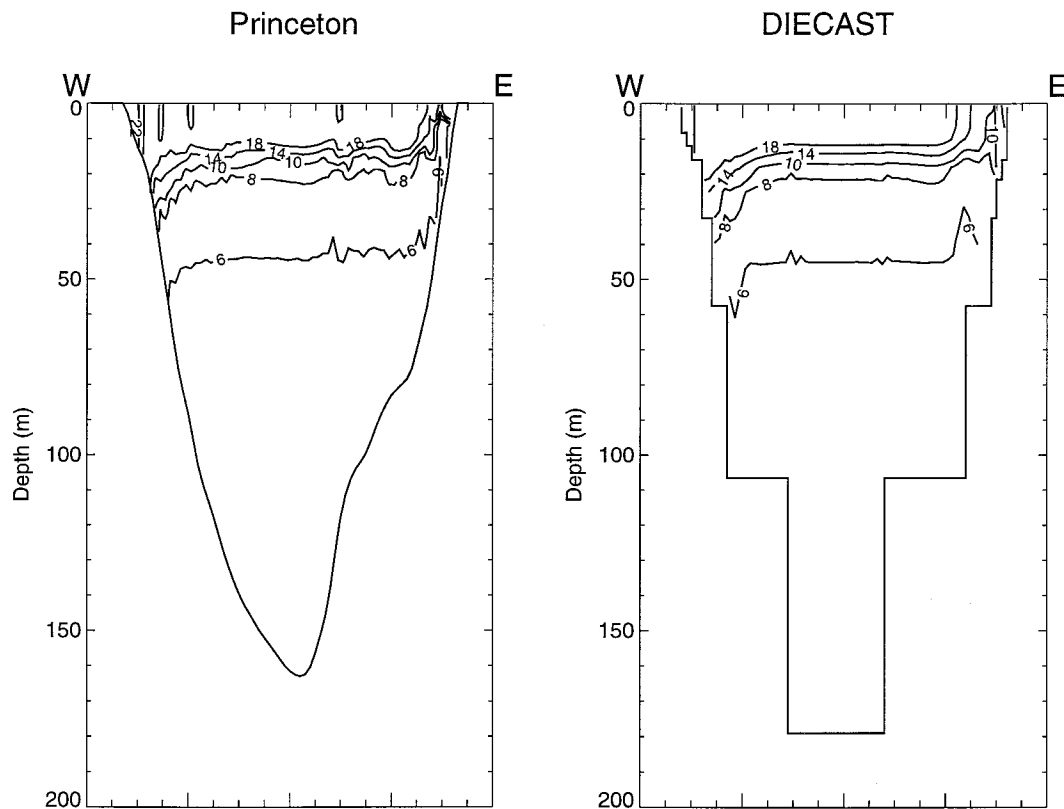


FIG. 15. East-west cross section at  $42.6^{\circ}\text{N}$  of temperature distribution at the moment of maximum upwelling (day 1.2) in the Lake Michigan case, 2-km grid.

## 5. Summary and discussion

We have applied two numerical ocean models that use essentially the same physics but significantly different numerical approaches to a case of coastal upwelling and Kelvin wave propagation in a circular basin and Lake Michigan. The physical differences between the models (free surface versus rigid lid, Mellor–Yamada versus Richardson number turbulence parameterization) are not significant for the upwelling–internal Kelvin wave problem. Although different finite differencing and vertical discretization schemes were used, the results of the two models were similar. Previously, little research has been done on three-dimensional Kelvin waves on the scale of large lakes. The Kelvin wave speed in both models is somewhat less than the inviscid linear wave speed for the flat-bottom circular lake case. This difference may be attributed to physical and numerical diffusion (Hsieh et al. 1983) in both models. In particular, Bennett (1977) also showed that the Kelvin wave speed is sensitive to the horizontal resolution of the model. In the full upwelling case, the frontal speed was practically equal to the wave speed from the light wind case for the DIECAST model. The POM results were more sensitive to grid resolution in the full upwelling case than in the light wind case. The Kelvin wave speed was faster in the circular lake with sloping

topography for both models. Vertical resolution was not as critical as horizontal resolution.

This study also contributes to resolving an intriguing problem in physical limnology. The majority of upwelling relaxation observations highlight the propagation of the warm front, and only up to a certain stagnation point (Mortimer 1963; Csanady 1977; Simons and Schertzer 1987). As noted in the circular lake tests, and in the Lake Michigan case, warm front propagation is more noticeable because of the sharp temperature increase in the time series records, while the cold front yields a much weaker signal. This characteristic might be the result of gravity acting to weaken a cold front stratification and maintain a warm front stratification. Incoming shortwave radiation will also mask cold front propagation. From the circular paraboloid results we also learned that Kelvin waves were able to propagate freely around the lake, but upwelling fronts were not because of the interaction with the geostrophic circulation over the sloping bottom. As Csanady (1977) mentioned, a similar situation was observed in Lake Ontario with upwelling along the northern shore when the thermocline front was shifted up to 14 km offshore in October 1972. There was no propagation of the cold front along the southern shore in the case of this very strong wind, but the propagation of a Kelvin wave was ob-

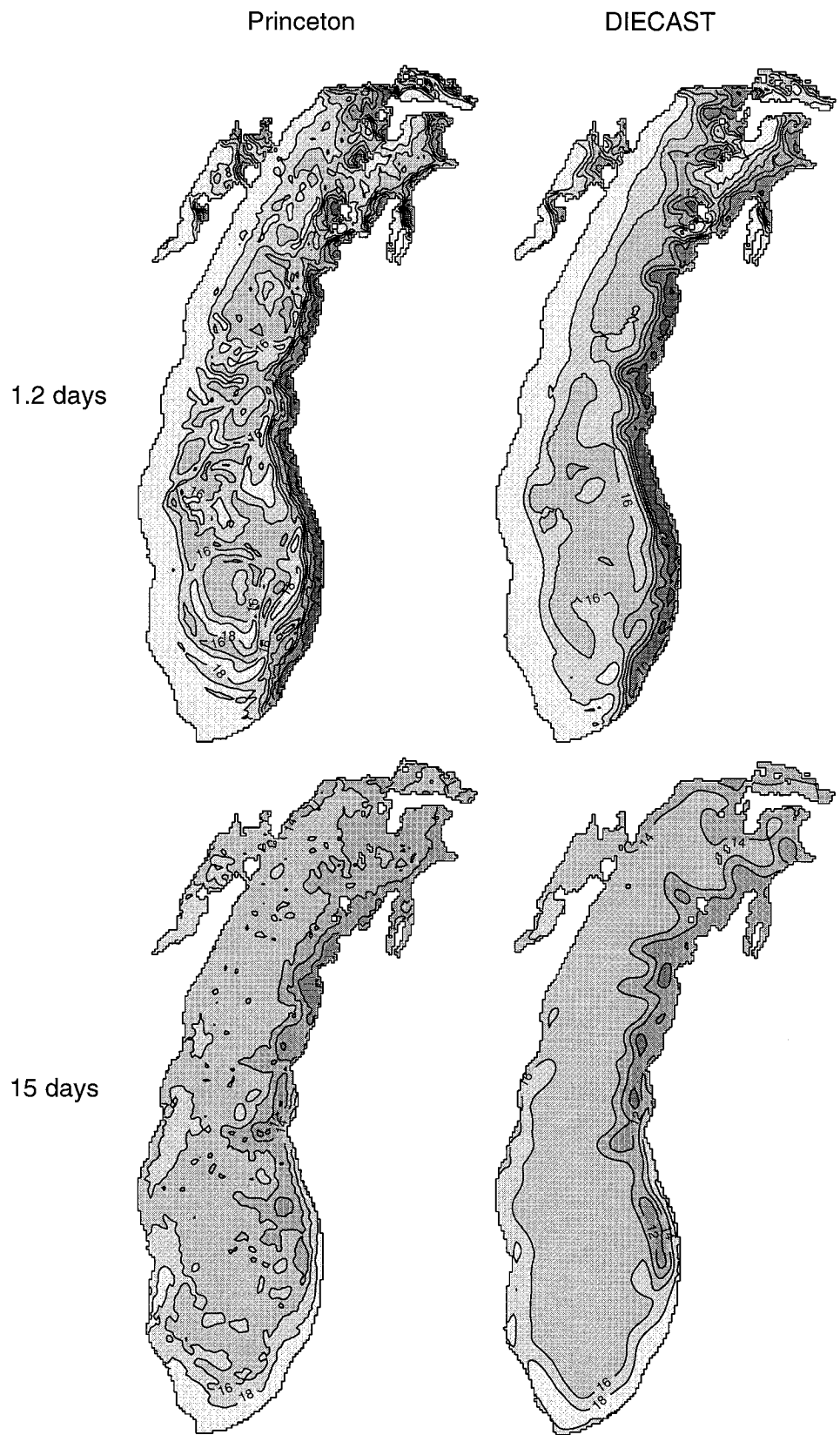


FIG. 16. Temperature at 13-m depth for Princeton and DIECAST models, 2-km grid.

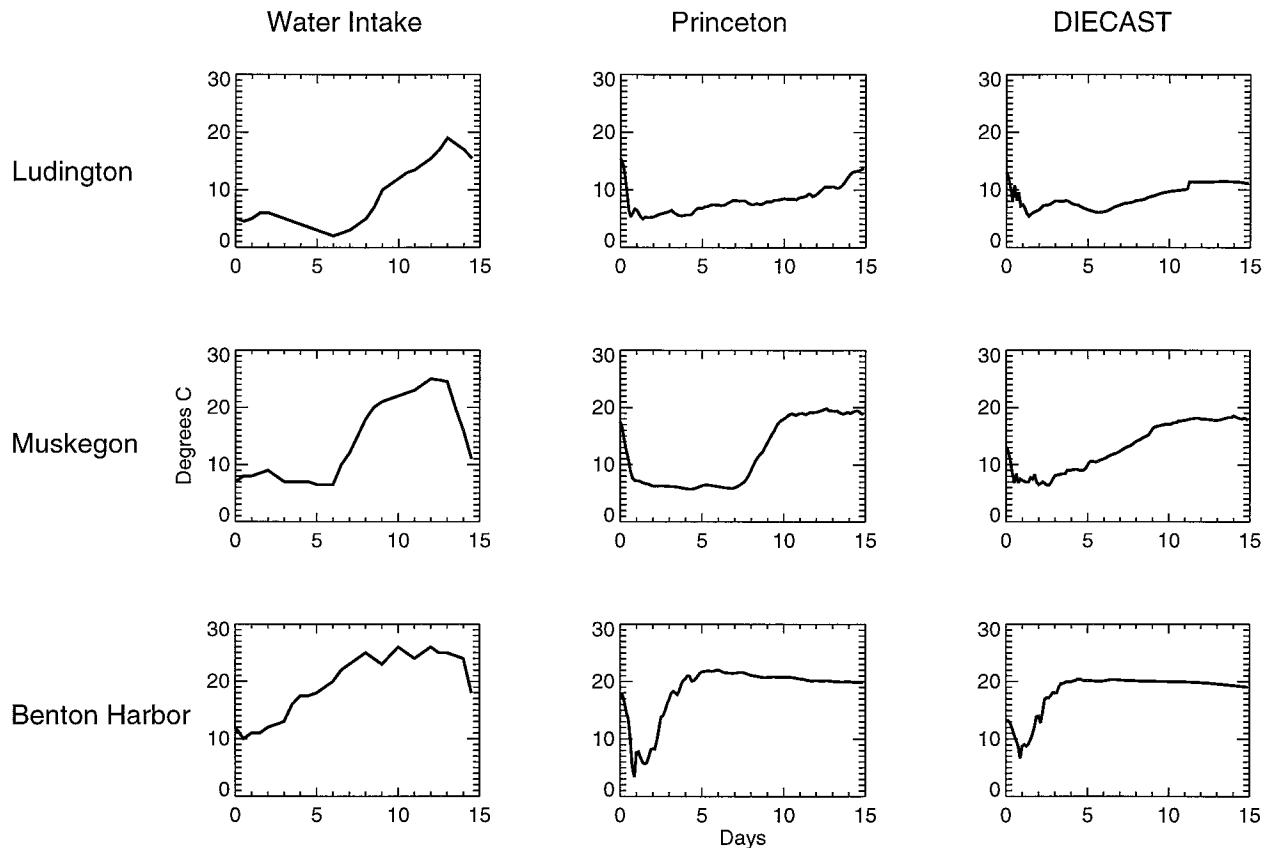


FIG. 17. Time series of 13-m temperature at Benton Harbor, Muskegon, and Ludington, Michigan (from Mortimer 1963), and results from Princeton and DIECAST models, 2-km grid.

served after much weaker wind forcing (and upwelling) earlier in July.

The relatively simple geometry of the circular paraboloid basin and simple wind forcing resulted in a complex response. This should be kept in mind when considering the response of a real lake to realistic winds. One can also expect the results for Lake Michigan to be different from those of the circular paraboloid basin because of the aspect ratio of the basin, differences in bathymetric slope, and coastal irregularities. Furthermore, the lake bathymetry is not duplicated exactly in the two models: the Lake Michigan bathymetry was filtered to remove steep gradients for the  $\sigma$ -coordinate model, and the bathymetry for the  $z$ -level model will change slightly depending on the levels chosen. Nevertheless, the results of the two different numerical models were remarkably similar both for the circular lake and for the Lake Michigan case studies. In fact, the results of the two models are closer to each other than they are to the observed results. We found that the frontal speeds in both models were less than the observed frontal speeds. The ability to accurately simulate upwelling and subsequent relaxation in a large lake also depends on knowledge of the initial three-dimensional temperature structure and temporal and spatial vari-

ability of the wind field. In order to better simulate the Lake Michigan upwelling case described above, it would be necessary to have more exact data, which are unavailable. Despite the problems mentioned, both models have demonstrated the ability to simulate complex physics with limited data. This qualitative agreement with observations gives us confidence in our ability to proceed with numerical modeling of the Great Lakes.

*Acknowledgments.* The authors express their thanks to M. J. McCormick, J. H. Saylor, K. M. Stewart, C.N.K. Mooers, and anonymous reviewers for their suggestions. The Richardson number turbulence parameterization subroutine for the DIECAST model was provided by P. J. Martin of the Naval Research Laboratory. The research was partially supported by the NOAA Coastal Ocean Program and the USEPA Lake Michigan Mass Balance Program. One author (DB) was supported by a fellowship from the Central European University, Budapest, Hungary.

#### REFERENCES

- Aikman, F., III, G. L. Mellor, T. Ezer, D. Sheinin, P. Chen, L. Breaker, K. Bosley, and D. B. Rao, 1996: Towards an operational nowcast/

- forecast system for the U.S. East Coast. *Modern Approaches to Data Assimilation in Ocean Modeling*, Oceanogr. Ser., Vol. 61, Elsevier, 347–376.
- Ayers, J. C., D. C. Chandler, G. H. Lauff, C. F. Powers, and E. B. Henson, 1958: Currents and water masses of Lake Michigan. Great Lakes Research Institute Publ. No. 3. 169 pp.
- Beletsky, D. V., N. N. Filatov, and R. A. Ibraev, 1994: Hydrodynamics of Lakes Ladoga and Onega. *Water Poll. Res. J. Canada*, **29**, 365–383.
- Bennett, J. R., 1973: A theory of large amplitude Kelvin waves. *J. Phys. Oceanogr.*, **3**, 57–60.
- , 1977: A three-dimensional model of Lake Ontario's summer circulation. I: Comparison with observations. *J. Phys. Oceanogr.*, **7**, 591–601.
- , and E. J. Lindstrom, 1977: A simple model of Lake Ontario's coastal boundary layer. *J. Phys. Oceanogr.*, **7**, 620–625.
- , and J. E. Campbell, 1987: Accuracy of a finite-difference method for computing lake currents. *J. Comput. Phys.*, **68**, 262–271.
- Blumberg, A. F., and G. L. Mellor, 1987: A description of a three-dimensional coastal ocean circulation model. *Three-Dimensional Coastal Ocean Models, Coastal and Estuarine Sciences*, Vol. 4, N. S. Heaps, Ed., Amer. Geophys. Union, 1–16.
- Bolgrien, D. W., and A. S. Brooks, 1992: Analysis of thermal features of Lake Michigan from AVHRR satellite images. *J. Great Lakes Res.*, **18**(2), 259–266.
- Boyce, F. M., M. A. Donelan, P. F. Hamblin, C. R. Murthy, and T. J. Simons, 1989: Thermal structure and circulation in the Great Lakes. *Atmos.–Ocean*, **27** (4), 607–642.
- Clarke, A. J., 1977: Observational and numerical evidence for wind-forced coastal trapped long waves. *J. Phys. Oceanogr.*, **7**, 231–247.
- Csanady, G. T., 1968: Wind-driven summer circulation in the Great Lakes. *J. Geophys. Res.*, **73** (8), 2579–2589.
- , 1977: Intermittent “full” upwelling in Lake Ontario. *J. Geophys. Res.*, **82**, 397–419.
- , 1984: *Circulation in the Coastal Ocean*. D. Reidel, 279 pp.
- , and J. T. Scott, 1974: Baroclinic coastal jets in Lake Ontario during IFYGL. *J. Phys. Oceanogr.*, **4**, 524–541.
- Davey, M. K., W. W. Hsieh, and R. C. Wajswowicz, 1983: The free Kelvin wave with lateral and vertical viscosity. *J. Phys. Oceanogr.*, **13**, 2182–2191.
- Dietrich, D. E., 1993: On modeling geophysical flows having low Rossby numbers. *Atmos.–Ocean*, **31**(1), 57–71.
- , 1997: Application of a modified Arakawa “a” grid ocean model having reduced numerical dispersion to the Gulf of Mexico circulation. *Dyn. Atmos. Oceans*, in press.
- , and D.-S. Ko, 1994: A semi-collocated ocean model based on the SOMS approach. *Int. J. Numer. Methods Fluids*, **19**, 1103–1113.
- , and C. A. Lin, 1994: Numerical studies of eddy shedding in the Gulf of Mexico. *J. Geophys. Res.*, **99**(C4), 7599–7615.
- , P. J. Roache, and M. G. Marietta, 1990: Convergence studies with the Sandia Ocean Modeling System. *Int. J. Numer. Methods Fluids*, **11**, 127–150.
- Haney, R. L., 1991: On the pressure gradient force over steep topography in sigma coordinate ocean models. *J. Phys. Oceanogr.*, **21**, 610–619.
- Heinrich, J., W. Lick, and J. Paul, 1981: Temperatures and currents in a stratified lake: A two-dimensional analysis. *J. Great Lakes Res.*, **7**(3), 264–275.
- Hsieh, W. W., M. K. Davey, and R. C. Wajswowicz, 1983: The free Kelvin wave in finite-difference models. *J. Phys. Oceanogr.*, **13**, 1383–1397.
- McCormick, M. J., and D. Scavia, 1981: Calculation of vertical profiles of lake-averaged temperature and diffusivity, in Lakes Ontario and Washington. *Water Resour. Res.*, **17**, 305–310.
- , and G. A. Meadows, 1988: An intercomparison of four mixed layer models in a shallow inland sea. *J. Geophys. Res.*, **93**(C6), 6774–6788.
- Mellor, G. L., 1991: An equation of state for numerical models of oceans and estuaries. *J. Atmos. Oceanic Technol.*, **8**, 609–611.
- , and T. Yamada, 1982: Development of a turbulence closure model for geophysical fluid problems. *Rev. Geophys. Space Phys.*, **20**(4), 851–875.
- Mooers, C. N. K., and J. Wang, 1996: Second-generation Straits of Florida nowcast/forecast system. Preprints, *Conf. on Coastal Oceanic and Atmospheric Prediction*, Atlanta, GA, Amer. Meteor. Soc., 28–35.
- Mortimer, C. H., 1963: Frontiers in physical limnology with particular reference to long waves in rotating basins. *Proc. Sixth Conf. Great Lakes Res.*, Great Lakes Res. Div., University of Michigan, Vol. 10, 9–42.
- , 1975: Part 1. Physical characteristics of Lake Michigan and its responses to applied forces. *Environmental Status of the Lake Michigan Region*, Vol. 2, *Physical Limnology of Lake Michigan*, Report ANL/ES-40, Argonne National Laboratory, 13–102.
- , 1988: Discoveries and testable hypotheses arising from Coastal Zone Color Scanner imagery of southern Lake Michigan. *Limnol. Oceanogr.*, **33**, 203–226.
- Murthy, C. R., and W. M. Schertzer, 1994: Physical limnology and water quality modeling of North American Great Lakes. Part I. Physical processes. *Water Poll. Res. J. Canada*, **29**, 129–156.
- O'Connor, W. P., and D. J. Schwab, 1994: Sensitivity of Great Lakes Forecasting System nowcasts to meteorological fields and model parameters. *Estuarine and Coastal Modeling III, Proc. Third Int. Conf.*, Oak Brook, IL, Amer. Soc. Civil Eng., 149–157.
- Rao, D. B., and B. C. Doughty, 1981: Instability of coastal currents in the Great Lakes. *Arch. Meteor. Geophys. Bioklimatol., Ser. A*, **30**, 145–160.
- Saylor, J. H., J. C. K. Huang, and R. O. Reid, 1980: Vortex modes in southern Lake Michigan. *J. Phys. Oceanogr.*, **10**, 1814–1823.
- Schwab, D. J., 1977: Internal free oscillations in Lake Ontario. *Limnol. Oceanogr.*, **22**, 700–708.
- , and D. L. Sellers, 1980: Computerized bathymetry and shorelines of the Great Lakes. NOAA Data Rep. ERL GLERL-16.
- , and K. W. Bedford, 1994: Initial implementation of the Great Lakes Forecasting System: A real-time system for predicting lake circulation and thermal structure. *Water Poll. Res. J. Canada*, **29**, 203–220.
- , W. P. O'Connor, and G. L. Mellor, 1995: On the net cyclonic circulation in large stratified lakes. *J. Phys. Oceanogr.*, **25**, 1516–1520.
- Simons, T. J., 1973: *Development of Three-Dimensional Numerical Models of the Great Lakes*. Can. Inland Waters Branch Sci. Ser., **12**, 26 pp.
- , and W. M. Schertzer, 1987: Stratification, currents and upwelling in Lake Ontario, summer 1982. *Can. J. Fish. Aquat. Sci.*, **44**, 2047–2058.
- Wajswowicz, R. C., and A. E. Gill, 1986: Adjustment of the ocean under buoyancy forces. Part I: The role of Kelvin waves. *J. Phys. Oceanogr.*, **16**, 2097–2114.
- Wang, D. P., 1982: Development of a three-dimensional, limited area (island) shelf circulation model. *J. Phys. Oceanogr.*, **12**, 605–617.
- , and C. N. K. Mooers, 1976: Coastal-trapped waves in a continuously stratified ocean. *J. Phys. Oceanogr.*, **6**, 853–863.
- Zuur, E. A. H., and D. E. Dietrich, 1990: The SOMS model and its application to Lake Neuchatel. *Aquat. Sci.*, **52**, 115–129.